coatings

MDPI

*Article*

# Enhancing the Corrosion Resistance of Low Pressure Cold Sprayed Metal Matrix Composite Coatings on AZ31B Mg Alloy through Friction Stir Processing

**Ashokkumar Mohankumar [1,*], Thirumalaikumarasamy Duraisamy [1], Ramachandran Chidambaramseshadri [2], Thirumal Pattabi [3], Sathiyamoorthy Ranganathan [4], Murugan Kaliyamoorthy [5], Guruprasad Balachandran [6], Deepak Sampathkumar [3] and Pradeep Raj Rajendran [7]**

1 Department of Manufacturing Engineering, Annamalai University, Annamalai Nagar 608002, India; tkumarasamy412@gmail.com
2 Department of Materials Science and Engineering, The State University of New York (SUNY) at Stony Brook, New York, NY 11794, USA; csrcn1@gmail.com
3 Department of Mechanical Engineering, Government College of Engineering, Krishnagiri 635104, India; ptm76@gmail.com (T.P.); naamphd@gmail.com (D.S.)
4 Department of Mechanical Engineering, Institute of Road Transport Polytechnic College, Krishnagiri 635104, India; rsmoorthy32@gmail.com
5 Department of Mechanical Engineering, Government Polytechnic College, Thiruvarur 612804, India; murugan.thermal@gmail.com
6 Department of Mechanical Engineering, Alagappa Chettiar Government College of Engineering and Technology, Karaikudi 630003, India; tellprasadcdm@gmail.com
7 Department of Mechanical Engineering, Mohandas College of Engineering and Technology, Trivandrum 695544, India; krsreeraj1@gmail.com
* Correspondence: ashokleadsaero12@gmail.com

**Abstract:** To improve the corrosion resistance of Mg alloy, Al alloy/alumina metal matrix composite (MMC) coatings were formed by low pressure cold spraying (LPCS) technology followed by post friction stir processing. The phase structure, microstructure, and corrosion properties of the cold-sprayed metal matrix composite coatings before and after friction stir processing were investigated. The effect of the friction stir process (FSP) on the corrosion characteristics of MMC coatings at 3.5 weight percent of NaCl solution was explored using a Tafel polarisation plot. Microstructural studies were examined to investigate the electrochemical behaviour of the cold spray (CS) and FSPed MMC coatings. The results demonstrated that an enhancement in corrosion protection of the MMC deposits occurred at the 1st and 2nd runs of FSP, with superior corrosion performance observed at the 2nd run of FSP. The enhanced surface state is the primary enhancement mechanism of the electrochemical properties of the FSPed MMC coatings. For the higher run of FSP (3rd run), the electrochemical performance of the specimens was lower owing to the amalgamate action of the enhanced surface state with the aggravated interface of interior deposits.

**Keywords:** cold spray; friction stir process; metal matrix composites; electrochemical behaviour

check for updates

**Citation:** Mohankumar, A.; Duraisamy, T.; Chidambaramseshadri, R.; Pattabi, T.; Ranganathan, S.; Kaliyamoorthy, M.; Balachandran, G.; Sampathkumar, D.; Rajendran, P.R. Enhancing the Corrosion Resistance of Low Pressure Cold Sprayed Metal Matrix Composite Coatings on AZ31B Mg Alloy through Friction Stir Processing. *Coatings* **2022**, *12*, 135. https://doi.org/10.3390/coatings12020135

Academic Editor: Mohammadreza Daroonparvar

Received: 5 November 2021
Accepted: 11 January 2022
Published: 24 January 2022



## 1. Introduction

Aluminium metal matrix composites (MCC) are actively employed in numerous fields like aerospace, marine, and automobile industries due to its great strength, excellent modulus of elasticity, and superior tribological properties [1–3]. MMCs produced using traditional processes such as liquid and powder metallurgy [2,4–7] and various thermal spray technologies [8,9] frequently have flaws like pores, larger grain size, weak bond strength, and undesired interfacial reaction products. However, the most developing technology is a solid-state coating method called "cold spray" (CS), which has been suggested to develop MMCs due to its lower processing temperature and high velocity capabilities [10–14].

Cold sprayed MMC coatings have less porosity and higher adhesive and cohesive strength among the metallic elements than cold sprayed raw metallic deposits [15,16]. Due to the presence of ceramic components, they can effectively permit metallic particles to deform plastically. Nevertheless, the cohesive strength is lower among the ceramic-metal and ceramic-ceramic components, which may also occur through cold sprayed MMC coatings. Significant cracks and micro or nano pores (unbounded regions) at these interfaces cause strong localised corrosion, which decreases the electrochemical performance of the deposits [17,18].

Some researchers have examined the electrochemical behaviour of cold sprayed aluminum-based MMC coatings through electrochemical techniques [18–28]. The electrochemical performance of the cold sprayed AA5056/SiC MMC deposit provided that the addition of SiC particles lowered the current rate at a potential of >600 mV [21]. But another study reveals the corrosion resistance of the cold spayed AA7075/SiC MMC deposit is lower in contrast to the cold sprayed pure AA7075 deposit. For cold sprayed MMC deposits, the domination of the massive plastically deformed metal elements or the existence of severely frail bonds affects the electrochemical behaviour of the coatings. Therefore, it is anticipated that corrosion protection of the coating may initially increase but then decrease as ceramic concentration increases [24]. It was discovered that Al with 70% and 30% alumina has superior corrosion resistance. As a result, optimising the ratio or dimension of the ceramic components would enhance the electrochemical behaviour of MMC coatings.

The commonly used post process method for cold sprayed deposits is heat treatment, which enhances bond strength as well as reduces the inter-particle boundary among the metallic particles that behave as preferred regions for corrosion [17,29,30]. Consequently, it is the suggested method for the electrochemical behaviour of cold sprayed raw metallic deposits [17]. Nevertheless, the impact of the cold sprayed MMC coatings is lower because they will not enhance the bond strength among the metal/ceramic elements through atomic diffusion. From this, there is a need to find post process techniques to increase the corrosion resistance of cold sprayed MMC deposits.

Friction stir processing (FSP) is a comparatively new technology with a wide range of surface modification possibilities [1,31–34]. The extreme plastic deformed state and the effect of raised stirred thermal energy [35–37] was developed through the friction stir process. Grain refinement and uniformly distributed reinforcing elements are attained. This leads to changes in surface microstructures and characteristics [32]. Previously, many researchers had explored using FSP to cold spray deposits [16,38–42]. The benefit of using the friction stir technique is that it enhances the tribological and erosion performance of cold sprayed composite coatings. Furthermore, earlier research suggests that FSP could be employed to enhance the mechanical behaviour of cold sprayed deposits [16,39]. The study proves that FSP improved the hardness of the cold gas dynamic sprayed AA7075 coating on the AZ31B substratum compared to as-sprayed coatings. This is due to the AA7075 deposit well refinement and the extreme plastic deformation produced by FSP [34].

From previous studies [1–58], it is evident that, to date, no research has been conducted to improve the corrosion performance of magnesium alloy using low pressure cold sprayed (LPCS) MMC coating by post process treatment.

Keeping the above point in mind, the present investigation was conducted to enhance the corrosion resistance of LPCSed MMC coatings on AZ31B Mg alloy through FSP.

The cold sprayed MMC coating and post-treat FSP may have remarkable refinement and redistribution of reinforcement particles and enhance the poor interface between the particles [16,31]. As a result, it has the potential to improve the electrochemical properties of cold sprayed MMC deposits. The aim of this research is to examine the practicability of using FSP to enhance the corrosion properties of LPCSed MMC coatings. To determine the impact of the FSP runs, a multi-run of FSP (with the first, second, and third runs) at 100% overlap is performed. The refining of alumina components and enhancement of inter-particle bonding, which majorly influences the corrosion performance of the Al alloy

matrix with dislocation density (DD) [43,44], would be analysed in order to explore the corrosion mechanisms.

## 2. Experimental Work

### *2.1. Manufacturing of MMC Coatings*

In this experiment, the feed stock powder was an Al alloy (grade: AA2024) (4.6 wt.% of Cu, 1.4 wt.% Mg, and Mn of 0.2 wt.%) with a particle size of 15 µm and an alumina of 20 µm. The two powders were blended using a ball milling process with 80 vol.% of Al alloy and 20 vol.% of alumina powder, as shown in Figure 1. AZ31B magnesium alloy (Al—3.0 wt.%, Mn—0.02 wt.%, Zn—1.0 wt.%, and Mg-balance) of 3 mm thickness was used as a base material. Before coating, the base materials were ground by abrasive sheets at a grit range of 1200 grit, washed by propane, and sandblasted (SEC-WB-9090, Sandstorm, Chennai, India). This was done with aluminium oxide (grit size of 300 ± 450 µm), morphology: blockish with fine edges, density of 2 g/cm$^3$, and hardness of 3 × 10$^4$ MPa. The MMC deposits were developed through the LPCS system (Dymet 423, Dymet, Tallinn, Estonia). According to the trial and error method and published literature review [1–58], the cold spray process parameters were optimised. These parameters provide the minimum porosity and maximum hardness of the coating. The optimised parameters were found through the Design of Experiment (DOE) using design expert software. Table 1 illustrates the optimised parameters of the LPCS process.

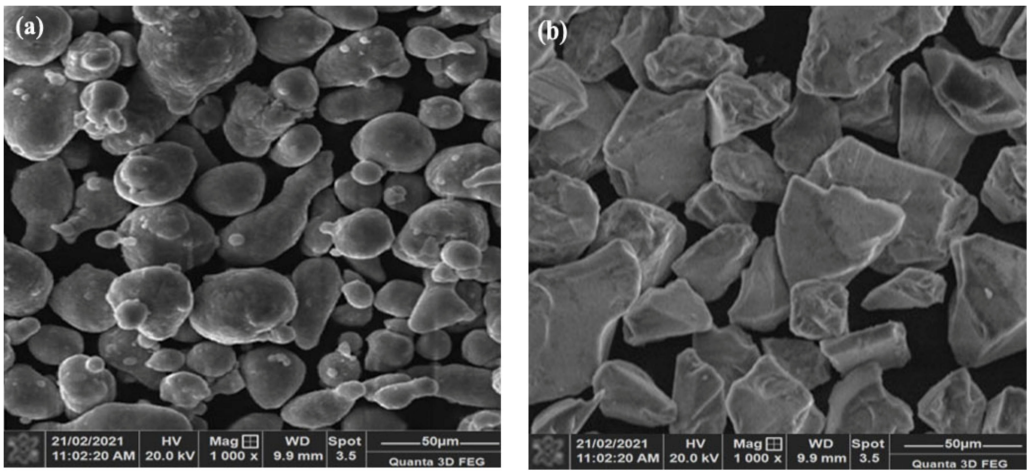


**Figure 1.** SEM images of coating material (**a**) Al alloy powder (**b**) Alumina powder.

**Table 1.** LPCS spray parameters.

| S. No | Parameters | Units | Ranges |
|---|---|---|---|
| 1 | Air pressure | bar | 12 |
| 2 | Air temperature | °C | 500 |
| 3 | Powder feed rate | g/min | 20 |
| 4 | Standoff distance | mm | 10 |

After LPCS, the post treatment was carried out on the surface of LPCSed MMC coatings with various runs (1st, 2nd, and 3rd runs). In this experiment, a friction stir welding machine (FSW RL54—090, RV Machine Tools, Chennai, India) was utilized as shown in Figure 2. A H13 steel stir-tool with a Vickers hardness of about 510 HV, a thread pin with a root diameter of 3.3 mm, a length of 2.8 mm, and a concave shoulder diameter of 10 mm was used in this equipment. The stir tool is inclined at a 2° elevation angle to eliminate surface flaws. The rotational orientation was counterclockwise at a rotational speed of 800 rpm with a traverse speed of 40 mm/min and a plunge depth of 2.8 mm for every run of FSP.

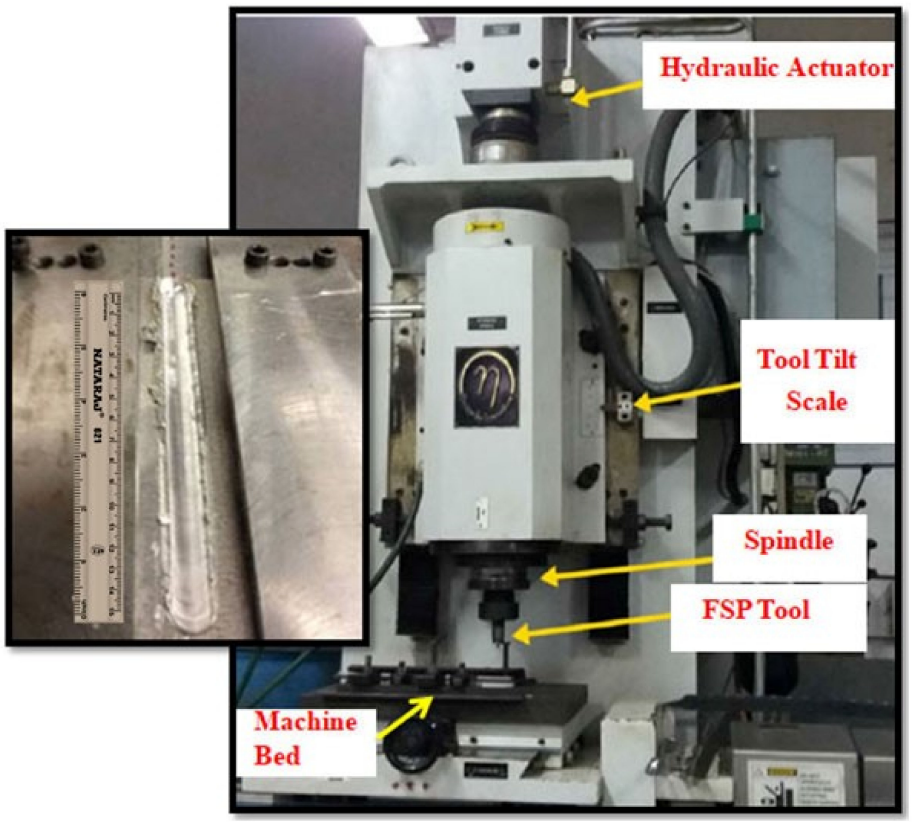


**Figure 2.** Friction stir processing setup.

### *2.2. Characterization of Materials*

The scanning electron microscope (SEM) (6410—LV, JEOL, Tokyo, Japan) was employed to examine the surface properties of the corroded specimens. The phase structural behaviour was determined using X-ray diffractometer equipment (XRD, ULTIMA-III, Rigaku, Tokyo, Japan) under Cu K$\alpha$ radiation at 23 °C. All XRD results were captured at a 2$\theta$ angle from 20 to 80° with a step resolution of 0.032°. For an LPCS sample, the hardness of the coating is measured using a Vickers hardness measurement system (HM-200, Mitutoyo, Tokyo, Japan), and the porosity of the deposit is estimated using an optical microscope (MIL—7100, Meiji, Tokyo, Japan) with image analysis software (Metal Vision, Version 6, 2016, Metavision Technology Pvt. Ltd, Bangalore, India).

### *2.3. Electrochemical Experiment*

The electrochemical experiments were conducted with the traditional three electrodes, as illustrated below.

- Reference as saturated calomel electrode (SCE),
- Counter as a platinum electrode,
- Working as MMC coatings.

The electrochemical performance of the LPCSed as well as FSPed samples was investigated through cyclic polarisation measurement at 3.5 wt.% NaCl solution at ambient temperature (23 °C) under neutral conditions with a scan speed of 0.34 mV/s. Before corrosion measurement, samples were polished and washed, and the operative circular region of the MMC electrode had a circumference of 4.9 mm. The open circuit potential (OCP) was measured at one hour, during which the samples were immersed in a 3.5 wt.% NaCl solution to maintain the samples in a static condition. The polarisation of the specimen was obtained in the range of −700 to 400 mV, which corresponds to the OCP. Then ZSimpWin

(3.2, 2019, Ametek Scientific Solution, Bangalore, India) software was used to study the spectral analysis.

## 3. Result and Discussion

### *3.1. Coating Microstructure and Characterization*

The optical microstructure view and XRD pattern of the Al alloy/alumina MMC coatings on AZ31B Mg alloy are shown in Figure 3a,b. From Figure 3a, it is inferred that the coating consists of deformed Al alloy and alumina particles. The first layer of coating is developed with greater adhesion between the substrate and coating due to the sandblasting process [19,24]. The adhesion strength of the coating was determined through a universal tensile testing machine (FIE02, Fuel Instruments and Engineers Pvt. Ltd., Chennai, India). The adhesion strength of the coating was about 48.2 MPa. Due to low processing temperatures [19,23,24], oxidation does not occur on the deposit. Due to low pressure process parameters [10,11], the metallurgical bonding between the interface of the matrix (Al alloy powder) and reinforcement (alumina) phase is not better. Numerous research studies arrived at the same results [3,19–24]. Figure 3b illustrates the XRD pattern of the coating. The peak shifting to a lower 2θ value indicates an expansion to a higher lattice parameter and the peaks confirm that the deposit is a metal matrix composite coating because the two peaks, aluminium and alumina, were found in the coating.

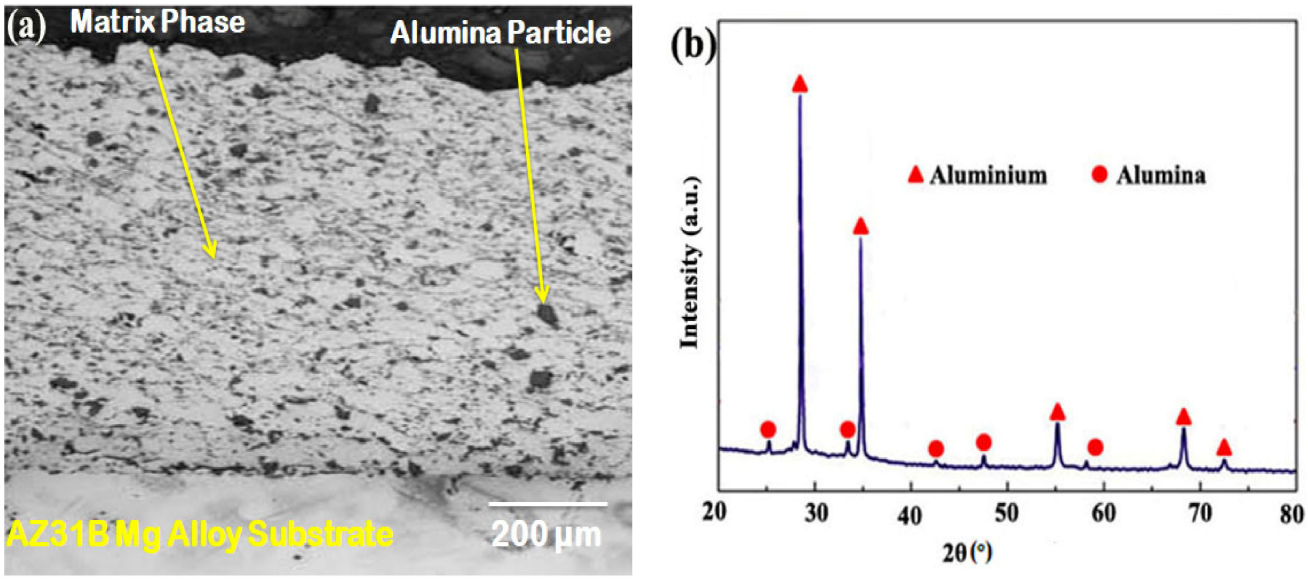


**Figure 3.** (**a**) Cross-sectional optical microstructure view (**b**) XRD of the LPCS MMC coatings.

Figure 4 illustrates cross-sectional SEM images of MMC coatings after the FSP process. From the figure, it is evident that the level of splitting and dispersion of alumina particles in the matrix phase rises after FSP due to the shearing force developed by the stirring motion of the tool on the coated sample.

The micro hardness measurement was conducted on the cross-section of the coated sample under a 250 g load with a 10 s holding span. The micro hardness of the coating was measured using a Vickers micro hardness tester at 15 different regions of the sample, and the average value was measured as 140 HV. The deposit reveals excellent hardness due to the presence of alumina particles in the deposit [19–22]. The optical microscope with image analysis software was utilised to examine the porosity of the coatings based on the ASTM B276 standards. The sample was metallographically (polished), developed, and etched. The images obtained with optical microscopy under 900× were selected for porosity evaluation to investigate the image properties like pores and a consistent pattern of cracks. A 500 micron square region was chosen on the deposit and the image was examined. The study was repeated five times in various regions to determine the average percentage

level of porosity, and the porosity of the as-sprayed coating was about 3%. After FSP, the porosity of the coatings was reduced to 1%. The thickness of the coatings was determined through a digital vernier calliper (0.001 mm accuracy) (CD-6CSX, Mitutoyo, Tokyo, Japan). The thickness of the as-sprayed coating was about 5 mm. After FSP, the thickness was about 1 mm.

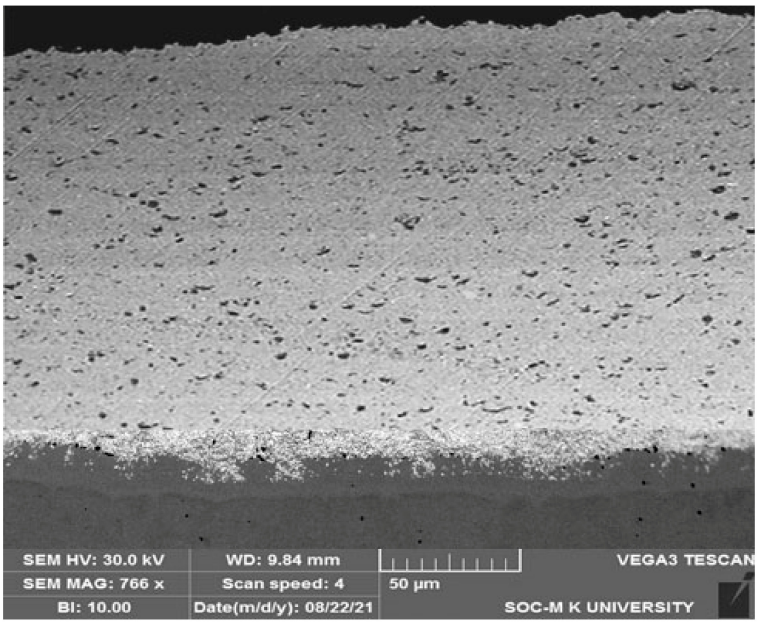


**Figure 4.** Cross-sectional SEM image after 2nd run of FSP.

### *3.2. Microstructural Study*

Refinement of Alumina Particles

The SEM photographs of the LPCSed and FSPed Al alloy/alumina coatings are shown in Figure 5. When compared with LPCSed samples, the level of splitting and dispersal of ceramic particles in the matrix phase rises after FSP, with some alumina particles retaining their earlier larger size. That is owing to the shearing force developed by the stirring motion of the tool on the coated samples. Then refining can result in enhanced mechanical properties due to a dispersal strengthening mechanism, as verified by previous research [16,31]. Although the continual disturbance of alumina particles formed during every run of FSP results in a decrease in their size, the higher the rise of FSP (3rd run), the breakage of ceramic particles becomes very small. The alumina particle size and dispersal levels of the second and third runs of FSPs are more or less equal, as shown in Figure 5c,d.

The alumina particle distribution became non-uniform after FSP, with increased degrees of splitting in both the upper and lower regions of the samples. This is owing to the flow of materials and stirring motion [31].

In comparison to bulk, the interfacial between the matrix and reinforcement phase in CSed deposits acts as a favourable location for corrosion [45–49]. Although the addition of alumina is expected to reduce the region that can be affected by an electrolytic solution of LPCSed MMCs, the impact can really be stronger around the alumina particles owing to the poor bond strength between the alumina particles and the matrix phase [18,22]. As a result, it has a low corrosive performance. Based on the previous study [1], extreme plastic deformation formed at the time of FSP has the ability to spread the alumina particles in the matrix phase as well as the capability to generate diffusion between the metallic components, thereby reducing the interparticle space among the particles. The outcome of space reduction between the particles and the refinement/redistribution of ceramic elements after FSP enhances the electrochemical behaviour of LPCSed Al alloy/alumina deposits.

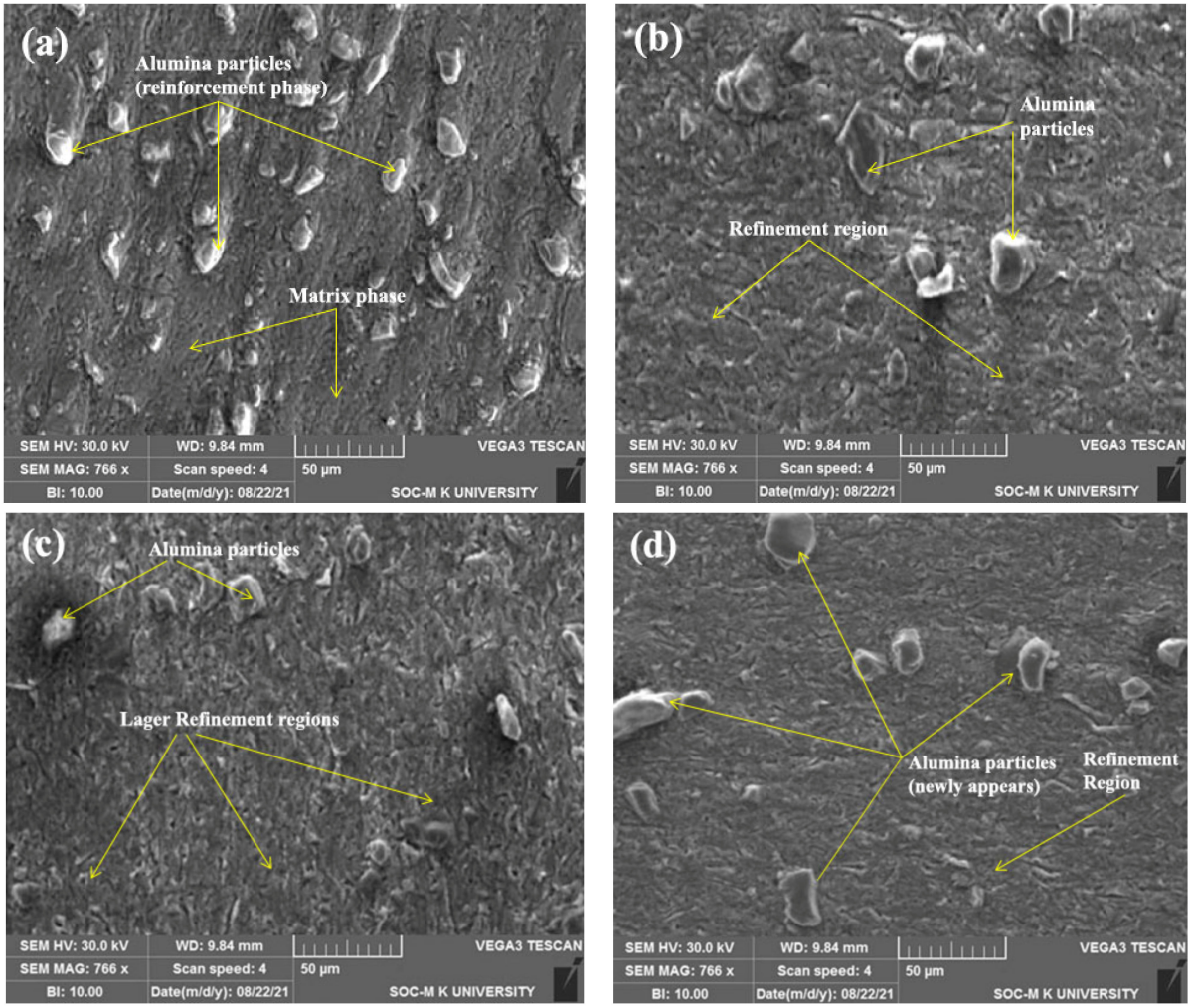


**Figure 5.** SEM images of (**a**) LPCS, (**b**) 1st, (**c**) 2nd, (**d**) 3rd runs of FSP.

### *3.3. Williamson–Hall Measurement*

Figure 6a depicts the XRD patterns of the LPCSed and FSPed samples. The XRD plot reveals that some of the peaks belong to the alumina elements in the FSPed samples, which have become smaller when compared with the LPCSed sample [50]. This is due to the lower size and higher levels of splitting between the alumina elements after FSP. The Williamson–Hall technique was utilised to find the Al alloy matrix dislocation density (DD) and micro strain (MS), as shown in Figure 6b. The results are illustrated in Table 2. [16,51,52]

$$d = k\lambda/(B\cos\theta) - (4\,\varepsilon\sin\theta) \quad (1)$$

$$\rho = \frac{2\sqrt{3}\left(\varepsilon^2\right)^{1/2}}{db} \quad (2)$$

Then the abbreviations for,

- k: Shape factor constant
- λ: X-ray wavelength
- d: Crystalline dimension
- ε: Lattice strain
- θ: Bragg angle
- ρ: Dislocation density
- b: Burgers vector
- B: Peak broadening width

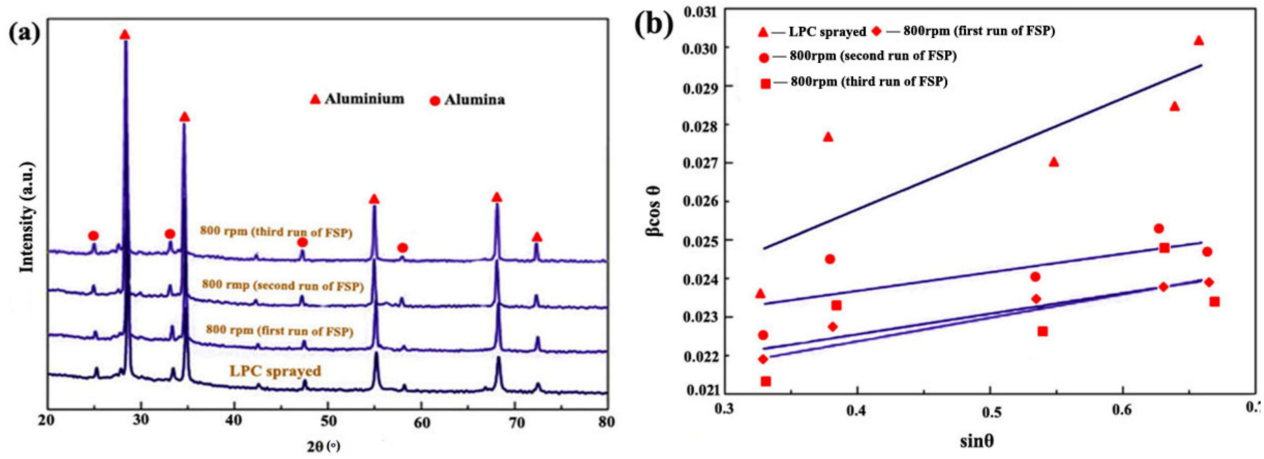


**Figure 6.** (**a**) XRD pattens of the LPC sprayed and FSPed samples and (**b**) Williamson—Hall graph.

From Equation (2), the values calculated are illustrated in Table 2. When compared with the LPCSed sample, the dislocation density and micro strain of the FSPed sample were very small. This is owing to the dynamic recrystallisation produced by the stir motion developed through FSP, as evidenced by multiple investigations. [53,54]. As a result of this, lower dislocation densities improve corrosion resistance [55,56]. Nevertheless, when MMC coatings are exposed to the 3rd run of FSP, higher dislocations are formed with severe micro strains but no effective breakup of the alumina particles. The 3rd run of FSP causes grain refinement as well as higher frequencies of greater angle grain boundaries [55,57], all of which negatively affect corrosion resistance.

**Table 2.** Results of dislocation density and micro strain.

| Samples | Crystalline Dimension (d) (nm) | Dislocation Density (ρ) ($mm^2$) | Micro Strain (ε) (%) |
|---|---|---|---|
| LPC Sprayed | 192.3 | $2.04 \times 10^{20}$ | 0.111 |
| 800 rpm (1st run of FSP) | 73.1 | $2.83 \times 10^{19}$ | 0.038 |
| 800 rpm (2nd run FSP) | 97.3 | $2.28 \times 10^{19}$ | 0.034 |
| 800 rpm (3rd run FSP) | 59.2 | $3.76 \times 10^{19}$ | 0.042 |

### *3.4. Corrosion Performance and Morphology*

The conventional cyclic polarisation of the LPCSed and FSPed MMC coatings at 3.5 wt.% NaCl solution is illustrated in Figure 7 (the red arrow represents the scanning orientation of the sample). At the time of ahead scanning, a passive area was detected at LPCSed and FSPed conditions, in which a passive protecting layer was developed. When the coated sample reaches the pitting potential ($E_{pit}$), the current density rises rapidly at a specific rate, and thereafter the potential rises at a moderate rate. At the time of backward scan, repassivity occurred at the repassivation potential ($E_{rp}$), corresponding with the potentials from which the polarisation curves intersect at backward scan. Figure 7 demonstrates the corrosion potential of the 2nd run of FSP. During this experiment, negative hysteresis loops were observed for all four corroded samples (corrosion potential greater than repassivation potential), which indicates the lower repassivity capacity of the samples and an adverse situation for pitting formation [45,46]. That is due to the significant energy stored in LPCSed and FSPed MMC coatings [45].

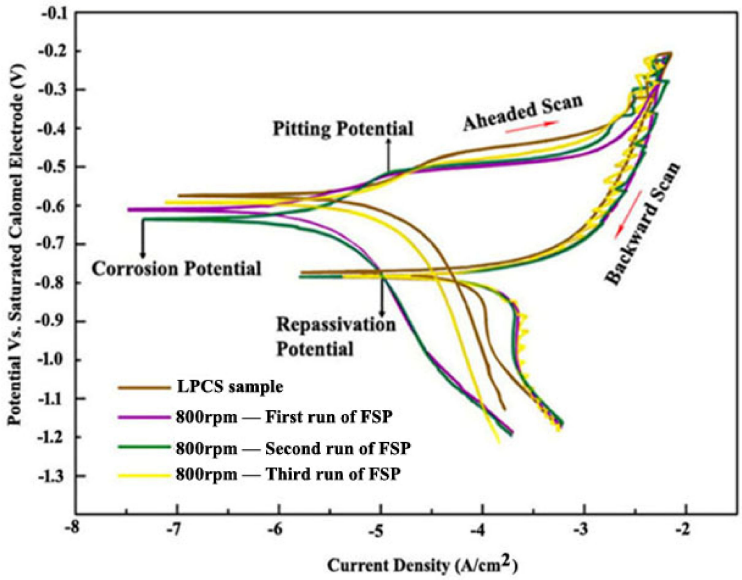


**Figure 7.** Tafel polarisation curves.

Table 3 illustrates the measured potentials of the cyclic polarisation plots. Differentiation between the pitting and corrosion potentials is a measurement of pitting nucleation. Whereas a greater differential indicates enhanced resistance to pitting corrosion. Similarly, the distinction between repassivation and corrosion potentials is related to repassivation capability [47,48]. Following successful completion of the 1st and 2nd runs of FSP, the differentiation between ($E_{pit}-E_{corr}$) and ($E_{rp}-E_{corr}$) is higher when compared with the LPCSed sample. As shown in Figure 8c,d, this indicates that the samples have improved repassivation capability and superior pitting corrosion resistance. The respective current densities of ($E_{corr}$, $E_{pit}$, and $E_{rp}$) of the first and second runs of the FSPed sample are obviously lower than those of the LPCSed sample. The comparison of the first and second runs of FSP revealed that the corrosion resistance of the second run was improved, as shown in Figure 8c,d, due to alumina element refining and redistribution, reduced space between the inter-splat boundary, re-oxidized aluminium phase on the surface, and reduced dislocation density in the matrix phase. Nevertheless, with higher runs of FSP (3rd runs), this difference reduces dramatically, pointing to a loss in corrosion behaviour as shown in Figure 8e. Because during FSP, after the 1st and 2nd run, a new layer of surface appears. In that layer, the interface bonding between the alumina particle and the matrix phase is poor and also FSP induces more grain refinement with higher frequencies of greater angle grain boundaries [54,57], which leads to poor corrosion behaviour on the sample.

**Table 3.** Outcome of Tafel polarisation analysis.

| Specimens | Current Densities | Potentials | | | | |
|---|---|---|---|---|---|---|
| | $I_{corr}$ ($A/cm^2$) | Corrosion ($V_{SCE}$) | Pitting ($V_{SCE}$) | Repassivation ($V_{SCE}$) | Pitting–Corrosion (V) | Repassivation–Corrosion (V) |
| LPC Sprayed | $1.31 \times 10^{-6}$ | −0.575 | −0.483 | −0.762 | 0.092 | −0.187 |
| 800 rpm (1st run of FSP) | $1.40 \times 10^{-7}$ | −0.612 | −0.517 | −0.780 | 0.095 | −0.168 |
| 800 rpm (2nd run FSP) | $1.21 \times 10^{-7}$ | −0.636 | −0.510 | −0.781 | 0.126 | −0.145 |
| 800 rpm (3rd run FSP) | $1.33 \times 10^{-6}$ | −0.594 | −0.504 | −0.777 | 0.090 | −0.183 |

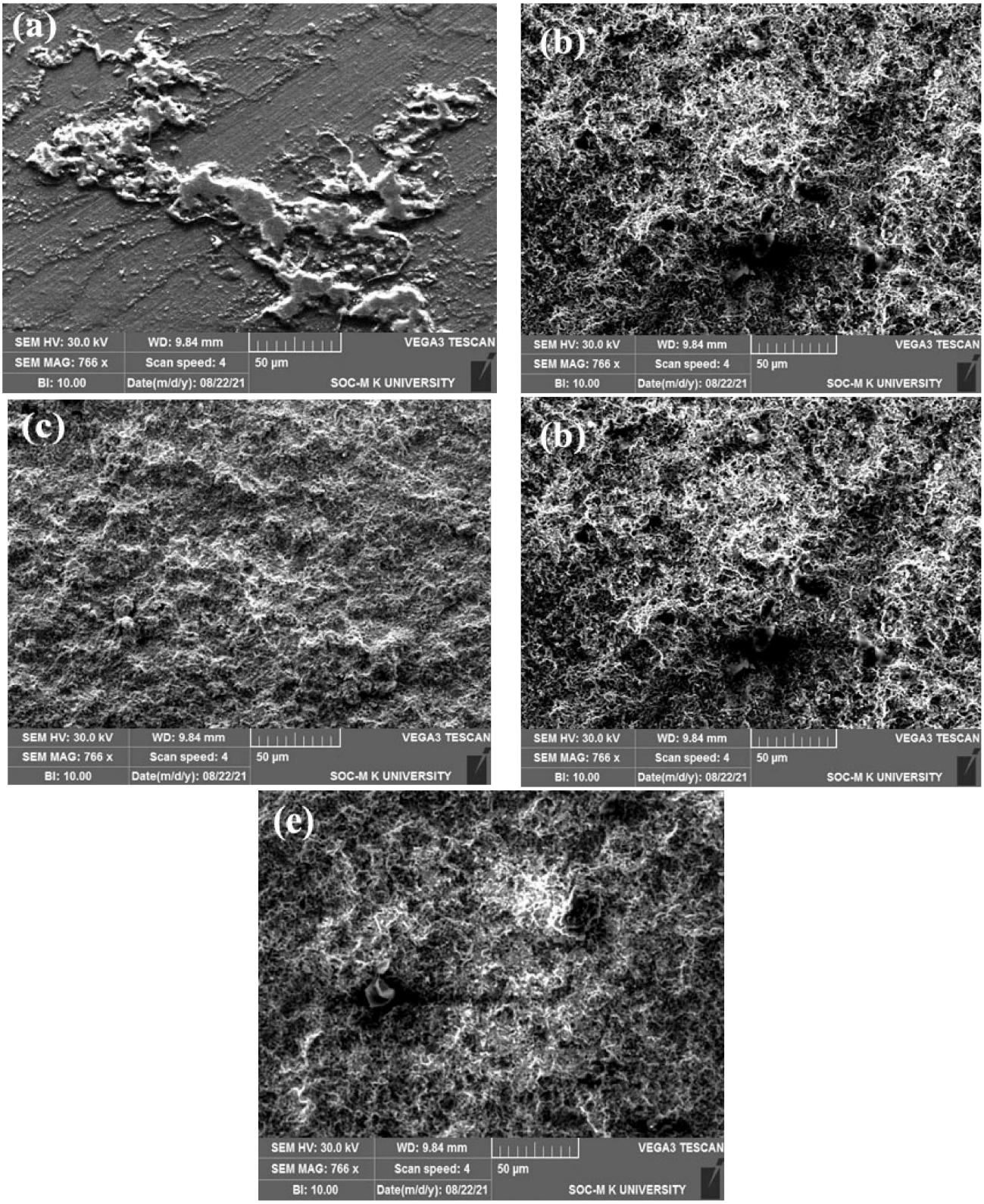


**Figure 8.** SEM morphology of corrosion performance of (**a**) AZ31B Mg alloy, (**b**) LPCSed; and (**c**) 1st, (**d**) 2nd, (**e**) 3rd runs of FSP after cyclic polarisation test.

### *3.5. Mechanism of Corrosion*

According to the FSPed, corrosion microstructure, and cyclic polarisation test outcomes, the corrosion performance of the LPCSed and FSPed MMC (Al alloy/Alumina) coatings were examined. Based on earlier research [18,45], the range of ($E_{pit}-E_{corr}$) and ($E_{rp}-E_{corr}$) influences the surface behaviour of deposits, such as flaws between particles and oxides of Al. After completion of FSP, the significantly enhanced surface state outcomes are measured by the rise of both ($E_{pit}-E_{corr}$) and ($E_{rp}-E_{corr}$) values. Based on the FSPed corrosion microstructural evaluation as shown in Figure 8, it is recommended to enhance the surface state of the FSPed Al alloy/Alumina due to: (i) the refinement/redistribution of the alumina element; (ii) the decrease in space between the inter-splat boundary; (iii) the re-oxidization of the aluminium phase on the surface; and (iv) the decrease in dislocation density in the matrix phase. However, at the higher run of FSP (3rd run), the dislocation density is increased due to newly formed coarse alumina particles and poor interface bonding between the matrix and reinforcement phase.

As shown in Figure 8e, weak interface states among the elements in the inner area of the deposits will be responsible for the reduction in corrosion resistance in the third run of FSP. This is due to the breakage of the oxide layer at the inner area of the coated Al alloy elements. During FSP aluminium phases are re-oxidized on the surface of the FSPed sample. At the higher run of FSP (3rd run), there is significant breakage of the oxide layers of the interior coated Al alloy elements and a reduction in protective performance. Previous investigations have proved the same behaviour [58]. FSP can enhance the surface state but also worsen the interior deposit of the FSP sample. To conclude, it can be inferred that the major enhancement mechanism of corrosion behaviour after the friction stir technique is the enhanced coating surface, which results in the rise of ($E_{pit}-E_{corr}$) and ($E_{rp}-E_{corr}$) values. At the lower run of FSP (1st and 2nd run), the values of ($E_{pit}-E_{corr}$) and ($E_{rp}-E_{corr}$) take a dominating position, resulting in improved corrosion resistance of the MMC deposit. At higher runs of FSP (3rd run), the ($E_{pit}-E_{corr}$) and ($E_{rp}-E_{corr}$) values do not reveal the better corrosion resistance compared to the 1st and 2nd runs of FSP. From this, the amalgamate action of the enhanced surface state and damaged interfaces of the interior deposits determined the disappointing corrosion behaviour.

## 4. Conclusions

The following are the conclusions that were attained:

(i) The size of the alumina components could be decreased by utilizing FSP. Multiple runs of FSP improved the rate of scattering and separation of alumina particles due to the high stir motion created by FSP.

(ii) The matrix phase (Al alloy) dislocation density and micro strain are lowered after the friction stir technique. The lower dislocation densities improve corrosion resistance. However, the dislocation density and micro strain were higher in the third run of FSP, which harmed corrosion resistance.

(iii) Furthermore, the lower (1st and 2nd) runs of FSP can significantly improve the protection against corrosion of the LPCSed Al alloy/alumina coating, and the 2nd run of FSP provides outstanding resistance to corrosion. The enhanced surface state is the primary enhancement mechanism for the FSPed MMC coatings.

(iv) The amalgamate action of the enhanced surface state and damaged interface of interior deposits would be accountable for the poor corrosion rate in the third run of the friction stir method.

(v) Changes in the weight percentages of aluminium alloy and alumina powder, as well as post-treatments such as laser remelting and heat treatment techniques, could be investigated further. The samples' corrosion performance must then be analyzed further using electrochemical impedance spectroscopy experiments.

**Author Contributions:** Conceptualization, A.M.; Data curation, S.R., D.S. and P.R.R.; Formal analysis, T.P., S.R. and P.R.R.; Funding acquisition, T.D., M.K. and G.B.; Investigation, A.M. and T.P.; Methodology, A.M.; Project administration, T.D. and T.P.; Resources, S.R. and D.S.; Software, S.R., M.K., G.B., D.S. and P.R.R.; Supervision, T.D.; Validation, R.C.; Visualization, D.S. and P.R.R.; Writing—original draft, A.M.; Writing—review & editing, T.D., T.P., S.R., D.S. and P.R.R. All authors have read and agreed to the published version of the manuscript.

**Funding:** The authors are grateful to the Department of Science and Technology (DST)-Science and Engineering Research Board (SERB), Government of India, New Delhi, for providing financial support for this study under the Empowerment and Equity Opportunities for Excellence in Science (EMEQ) scheme, R&D project File No. EEQ/2018/000472.

**Institutional Review Board Statement:** Not applicable.

**Informed Consent Statement:** Not applicable.

**Data Availability Statement:** Data sharing is not applicable to this article.

**Conflicts of Interest:** The authors declare no conflict of interest.

## References

1. Gangil, N.; Siddiquee, A.N.; Maheshwari, S. Aluminium based in-situ composite fabrication through friction stir processing: A review. *J. Alloys Compd.* **2017**, *715*, 91–104. [CrossRef]
2. Ashokkumar, M.; Thirumalaikumarasamy, D.; Thirumal, P.; Barathiraja, R. Influences of Mechanical, Corrosion, erosion and tribological performance of cold sprayed Coatings A review. *Mater. Today Proc.* **2021**, *46*, 7581–7587. [CrossRef]
3. Sharifitabar, M.; Sarani, A.; Khorshahian, S.; Afarani, M.S. Fabrication of 5052Al/Al2O3 nanoceramic particle reinforced composite via friction stir processing route. *Mater. Des.* **2011**, *32*, 4164–4172. [CrossRef]
4. Pan, J.; Li, J.H.; Fukunaga, H.; Ning, X.G.; Ye, H.Q.; Yao, Z.K.; Yang, D.M. Microstructural study of the interface reaction between whiskers and aluminium. *Compos. Sci. Technol.* **1977**, *57*, 319–325. [CrossRef]
5. Ramesh, C.; Pramod, S.; Keshavamurthy, R. A study on microstructure and mechanical properties of Al 6061–TiB2 in-situ composites. *Mater. Sci. Eng. A* **2011**, *528*, 4125–4132. [CrossRef]
6. Kumar, A.V. Method of stir casting of aluminum metal matrix composites: A review. *Mater. Today* **2017**, *4*, 1140–1146.
7. Chianeh, V.A.; Hosseni, H.R.M.; Nofar, N. Microstructural features and mechanical properties of Al-Al3Ti composite fabricated by in-situ powder metallurgy route. *J. Alloys Compd.* **2009**, *473*, 127–132. [CrossRef]
8. Yan, D.-R.; Yang, Y.; Chu, Z.-H.; Chen, X.-G.; Dai, X.-R.; Wang, Y.-H.; Dong, Y.-C. In situ composite coatings prepared by complex reactive plasma spraying of $Fe_2O_3$-Al-$Cr_2O_3$ composite powders. *Surf. Coat. Technol.* **2017**, *328*, 94–101. [CrossRef]
9. Mathanbabu, M.; Thirumalaikumarasamy, D.; Thirumal, P.; Ashokkumar, M. Study on thermal, mechanical, microstructural properties and failure analyses of lanthanum zirconate based thermal barrier coatings: A review. *Mater. Today Proc.* **2021**, *46*, 7948–7954. [CrossRef]
10. Assadi, H.; Kreye, H.; Gärtner, F.; Klassen, T. Cold spraying—A materials perspective. *Acta. Mater.* **2016**, *116*, 382–407. [CrossRef]
11. Lee, C.; Kim, J. Microstructure of Kinetic Spray Coatings: A Review. *J. Therm. Spray Technol.* **2015**, *24*, 592–610. [CrossRef]
12. Bashirzadeh, M.; Azarmi, F.; Leither, C.P.; Karami, G. Investigation on relationship between mechanical properties and microstructural characteristics of metal matrix composites fabricated by cold spraying technique. *Appl. Surf. Sci.* **2013**, *275*, 208–216. [CrossRef]
13. Yin, S.; Xie, Y.; Cizek, J.; Ekoi, E.J.; Hussain, T.; Dowling, D.P.; Lupoi, R. Advanced diamond- reinforced metal matrix com-posites via cold spray: Properties and deposition mechanism. *Compos. Part B-Eng.* **2017**, *113*, 44–54. [CrossRef]
14. Zhang, Y.; Wang, Q.; Ye, R.; Ramachandran, C.S. Plasma electrolytic oxidation of cold spray kinetically metallized CNT-Al coating on AZ91-Mg alloy: Evaluation of mechanical and surficial characteristics. *J. Alloys Compd.* **2021**, *892*, 162094. [CrossRef]
15. Yu, M.; Suo, X.K.; Li, W.Y.; Wang, Y.Y.; Liao, H.L. Microstructure, mechanical property and wear performance of cold sprayed Al5056/SiCp composite coatings: Effect of reinforcement content. *Appl. Surf. Sci.* **2014**, *289*, 188–196. [CrossRef]
16. Yang, K.; Li, W.; Niu, P.; Yang, X.; Xu, Y. Cold sprayed AA2024/$Al_2O_3$ metal matrix composites improved by friction stir processing: Microstructure characterization, mechanical performance and strengthening mechanisms. *J. Alloys Compd.* **2018**, *736*, 115–123. [CrossRef]
17. Hassani-Gangaraj, S.M.; Moridi, A.; Guagliano, M. Critical review of corrosion protection by cold spray coatings. *Surf. Eng.* **2015**, *31*, 803–815. [CrossRef]
18. Da Silva, F.S.; Bedoya, J.; Dosta, S.; Cinca, N.; Cano, I.; Guilemany, J.M.; Benedetti, A. Corrosion characteristics of cold gas spray coatings of reinforced aluminum deposited onto carbon steel. *Corros. Sci.* **2017**, *114*, 57–71. [CrossRef]
19. Spencer, K.; Fabijanic, D.M.; Zhang, M.X. The use of Al-Al2O3 cold spray coatings to improve the surface properties of magnesium alloys. *Surf. Coat. Technol.* **2009**, *204*, 336–344. [CrossRef]
20. Tao, Y.; Xiong, T.; Sun, C.; Jin, H.; Du, H.; Li, T. Effect of α-Al2O3 on the properties of cold sprayed Al/α-Al2O3 composite coatings on AZ91D magnesium alloy. *Appl. Surf. Sci.* **2009**, *256*, 261–266. [CrossRef]

21. Koivuluoto, H.; Vuoristo, P. Effect of Ceramic Particles on Properties of Cold-Sprayed Ni-20Cr+Al2O3 Coatings. *J. Therm. Spray Technol.* **2009**, *18*, 555–562. [CrossRef]
22. Wang, Y.; Normand, B.; Mary, N.; Yu, M.; Liao, H. Microstructure and corrosion behavior of cold sprayed SiCp/Al 5056 composite coatings. *Surf. Coat. Technol.* **2014**, *251*, 264–275. [CrossRef]
23. Meydanoglu, O.; Jodoin, B.; Kayali, E.S. Microstructure, mechanical properties and corrosion performance of 7075 Al matrix ceramic particle reinforced composite coatings produced by the cold gas dynamic spraying process. *Surf. Coat. Technol.* **2013**, *235*, 108–116. [CrossRef]
24. Irissou, E.; Legoux, J.-G.; Arsenault, B.; Moreau, C. Investigation of Al-Al2O3 Cold Spray Coating Formation and Properties. *J. Therm. Spray Technol.* **2007**, *16*, 661–668. [CrossRef]
25. Rao, Y.; Wang, Q.; Oka, D.; Ramachandran, C.S. On the PEO treatment of cold sprayed 7075 aluminum alloy and its effects on mechanical, corrosion and dry sliding wear performances thereof. *Surf. Coat. Technol.* **2019**, *383*, 125271. [CrossRef]
26. Rao, Y.; Wang, Q.; Chen, J.; Ramachandran, C.S. Abrasion, sliding wear, corrosion, and cavitation erosion characteristics of a duplex coating formed on AZ31 Mg alloy by sequential application of cold spray and plasma electrolytic oxidation techniques. *Mater. Today Commun.* **2020**, *26*, 101978. [CrossRef]
27. Zhang, Y.; Wang, Q.; Chen, G.; Ramachandran, C.S. Mechanical, tribological and corrosion physiognomies of CNT-Al metal matrix composite (MMC) coatings deposited by cold gas dynamic spray (CGDS) process. *Surf. Coat. Technol.* **2020**, *403*, 126380. [CrossRef]
28. Luo, X.; Chidambaram-Seshadri, R.; Yang, G.J. Micro-nanostructured cermet coatings. In *Advanced Nanomaterials and Coatings by Thermal Spray*; Elsevier: Amsterdam, The Netherlands, 2019; pp. 61–117.
29. Huang, R.; Sone, M.; Ma, W.; Fukanuma, H. The effects of heat treatment on the mechanical properties of cold-sprayed coatings. *Surf. Coat. Technol.* **2015**, *261*, 278–288. [CrossRef]
30. Yang, K.; Li, W.; Guo, X.; Yang, X.; Xu, Y. Characterizations and anisotropy of cold-spraying additive-manufactured copper bulk. *J. Mater. Sci. Technol.* **2018**, *34*, 1570–1579. [CrossRef]
31. Yang, K.; Li, W.; Huang, C.; Yang, X.; Xu, Y. Optimization of cold-sprayed AA2024/Al2O3 metal matrix composites via friction stir processing: Effect of rotation speeds. *J. Mater. Sci. Technol.* **2018**, *34*, 2167–2177. [CrossRef]
32. Ma, Z. Friction Stir Processing Technology: A Review. *Met. Mater. Trans. A* **2008**, *39*, 642–658. [CrossRef]
33. Mishra, R.; Ma, Z.; Charit, I. Friction stir processing: A novel technique for fabrication of surface composite. *Mater. Sci. Eng. A* **2003**, *341*, 307–310. [CrossRef]
34. Khodabakhshi, F.; Marzbanrad, B.; Shah, L.; Jahed, H.; Gerlich, A. Friction-stir processing of a cold sprayed AA7075 coating layer on the AZ31B substrate: Structural homogeneity, microstructures and hardness. *Surf. Coat. Technol.* **2017**, *331*, 116–128. [CrossRef]
35. Yang, C. A novel uncertainty-oriented regularization method for load identification. *Mech. Syst. Signal Process.* **2021**, *158*, 107774. [CrossRef]
36. Yang, C.; Hou, X.; Chang, S. A synchronous placement and size-based multi-objective optimization method for heat dissipation design on antenna module of space solar power satellite. Sustain. *Energy Technol. Assess.* **2021**, *45*, 101183. [CrossRef]
37. Yang, C.; Hou, X. Iterative two-layer thermal design strategy for step sandwich antenna of space solar power satellite using modified constrained multi-objective optimization. *Aerosp. Sci. Technol.* **2021**, *118*, 106987. [CrossRef]
38. Hodder, K.; Izadi, H.; McDonald, A.; Gerlich, A. Fabrication of aluminum–alumina metal matrix composites via cold gas dynamic spraying at low pressure followed by friction stir processing. *Mater. Sci. Eng. A* **2012**, *556*, 114–121. [CrossRef]
39. Huang, C.; Li, W.; Feng, Y.; Xie, Y.; Planche, M.-P.; Liao, H.; Montavon, G. Microstructural evolution and mechanical properties enhancement of a cold-sprayed Cu Zn alloy coating with friction stir processing. *Mater. Charact.* **2017**, *125*, 76–82. [CrossRef]
40. Huang, C.; Li, W.; Feng, Y.; Xie, Y.; Planche, M.P.; Liao, H.; Montavon, G. Modification of a cold sprayed SiCp/Al5056 composite coating by friction stir processing. *Surf. Coat. Technol.* **2016**, *296*, 69–75. [CrossRef]
41. Peat, T.; Galloway, A.; Toumpis, A.; Steel, R.; Zhu, W.; Iqbal, N. Enhanced erosion performance of cold spray co-deposited AISI316 MMCs modified by friction stir processing. *Mater. Des.* **2017**, *120*, 22–35. [CrossRef]
42. Peat, T.; Galloway, A.; Toumpis, A.; McNutt, P.; Iqbal, N. The erosion performance of cold spray deposited metal matrix composite coatings with subsequent friction stir processing. *Appl. Surf. Sci.* **2017**, *396*, 1635–1648. [CrossRef]
43. Pang, J.; Liu, F.; Liu, J.; Tan, M.-J.; Blackwood, D. Friction stir processing of aluminium alloy AA7075: Microstructure, surface chemistry and corrosion resistance. *Corros. Sci.* **2016**, *106*, 217–228. [CrossRef]
44. Alexopoulos, N.D.; Velonaki, Z.; Stergiou, C.I.; Kourkoulis, S.K. The effect of artificial ageing heat treatments on the corro-sion-induced hydrogen embrittlement of 2024 (Al-Cu) aluminium alloy. *Corros. Sci.* **2016**, *102*, 413–424. [CrossRef]
45. Kumar, S.; Jyothirmayi, A.; Wasekar, N.; Joshi, S. Influence of annealing on mechanical and electrochemical properties of cold sprayed niobium coatings. *Surf. Coat. Technol.* **2016**, *296*, 124–135. [CrossRef]
46. Xu, W.; Liu, J.; Zhu, H. Pitting corrosion of friction stir welded aluminum alloy thick plate in alkaline chloride solution. *Electrochim. Acta* **2010**, *55*, 2918–2923. [CrossRef]
47. Tao, Y.; Xiong, T.; Sun, C.; Kong, L.; Cui, X.; Li, T.; Song, G.L. Microstructure and corrosion performance of a cold sprayed aluminium coating on AZ91D magnesium alloy. *Corros. Sci.* **2010**, *52*, 3191–3197. [CrossRef]
48. Bai, Y.; Wang, Z.H.; Li, X.B.; Huang, G.S.; Li, C.X.; Li, Y. Corrosion behavior of low pressure cold sprayed Zn-Ni composite coatings. *J. Alloys Compd.* **2017**, *719*, 194–202. [CrossRef]

49. Ngai, S.; Ngai, T.; Vogel, F.; Story, W.; Thompson, G.B.; Brewer, L.N. Saltwater corrosion behavior of cold sprayed AA7075 aluminum alloy coatings. *Corros. Sci.* **2018**, *130*, 231–240. [CrossRef]
50. Barouz, M.; Givi, M.K.B. Fabrication of in situ Cu/SiC composites using multipass friction stir processing: Evaluation of microstructural, porosity, mechanical and electrical behaviour. *Compos. Part A Appl. Sci. Manuf.* **2011**, *42*, 1445–1453. [CrossRef]
51. Williamson, G.K.; Hall, W.H. X-ray line broadening from filed aluminium and wolfram. *Acta Metall.* **1953**, *1*, 22–31. [CrossRef]
52. Parmar, V.; Changela, K.; Srinivas, B.; Sankar, M.M.; Mohanty, S.; Panigrahi, S.K.; Hariharan, K.; Kalyanasundaram, D. Relationship between Dislocation Density and Antibacterial Activity of Cryo-Rolled and Cold-Rolled Copper. *Materials* **2019**, *12*, 200. [CrossRef] [PubMed]
53. Zhang, Z.; Li, W.; Feng, Y.; Li, J.; Chao, Y. Global anisotropic response of friction stir welded 2024 aluminum sheets. *Acta Mater.* **2015**, *92*, 117–125. [CrossRef]
54. Sato, Y.S.; Kokawa, H.; Enomoto, M.; Jogan, S. Microstructural evolution of 6063 aluminum during friction-stir welding. *Met. Mater. Trans. A* **1999**, *30*, 2429–2437. [CrossRef]
55. Rahsepar, M.; Jarahimoghadam, H. The influence of multipass friction stir processing on the corrosion behavior and mechanical properties of zircon-reinforced Al metal matrix composites. *Mater. Sci. Eng. A* **2016**, *671*, 214–220. [CrossRef]
56. Pandey, V.; Singh, J.K.; Chattopadhyay, K.; Srinivas, N.C.S.; Singh, V. Influence of ultrasonic shot peening on corrosion behavior of 7075 aluminum alloy. *J. Alloys Compd.* **2017**, *723*, 826–840. [CrossRef]
57. Sattari, B.; Shamanian, M.; Ashrafi, A.; Salehi, M.; Salimijazi, F. Effect of number of passes on the corrosion behavior of Fe/Al surface composites produced by plasma spraying and friction stir processing. *J. Mater. Process. Technol.* **2017**, *250*, 35–44. [CrossRef]
58. Niu, P.; Li, W.; Zhang, Z.; Wang, F.; Feng, Y.; Fu, M. Significant effect of oxide on mechanical properties of friction-stir-welded AA2024 joints. *Sci. Technol. Weld. Join.* **2016**, *22*, 66–70. [CrossRef]